Solar Energy 289 (2025) 113326

Contents lists available at ScienceDirect

Solar Energy

journal homepage: www.elsevier.com/locate/solener

Performance evaluation of a folded mini-channel heat sink for solar cell cooling: Experimental study

Amel Djebara [a], Nabil Bessanane [b], Mohamed Si-Ameur [b,*], Adnan Ibrahim [c,*], Zouheyr Noui [a], Sharul Sham Dol [d], Hariam Luqman Azeez [c], Sidi Ali Amira [a]

[a] University of Batna 2, LESEI laboratory ,Faculty of Technology, Electrical Department, 05000 Batna, Algeria
[b] University of Batna 2, LESEI laboratory, Faculty of Technology, Mechanical Department, 05000 Batna, Algeria
[c] Solar Energy Research Institute, Universiti Kebangsaan Malaysia, Bangi 43600, Malaysia
[d] Department of Mechanical and Industrial Engineering, Abu Dhabi University, Abu Dhabi PO Box 59911, United Arab Emirates

ARTICLE INFO

Keywords:
Low concentration photovoltaics (LCPV)
Folded fin mini-channel heat sink
Enhanced heat dissipation
Solar Cell Cooling
Photovoltaic efficiency improvement

ABSTRACT

This study addresses the critical challenge of reducing operating temperature in photovoltaic (PV) systems, as excessive heat generation impairs their electrical efficiency and power output. A novel mini-channel heat sink with a folded U-shaped fin design is introduced to enhance heat dissipation, offering a scalable solution for optimizing PV performance. The design increases the heat transfer area while reducing airflow velocity by narrowing the channels, and optimizing thermal management. Experiments were conducted indoors under controlled conditions, with inlet air velocity of 0.3, 0.6, 0.8, and 1 m/s and solar irradiances of 500 and 1000 W/m^2. The outcomes showed that the mini-channel heat sink effectively reduced the average cell temperature by 57.44 %. This significant thermal regulation increased electrical efficiency by 26.6 %, resulting in a 37.55 % increment in power output. The experimental findings were further compared to numerical simulations achieving an acceptable range of variation and ensuring the reliability of the results with an average heat transfer coefficient error percentage below 5 %. The originality of this work lies then in its unique U-shaped mini-channel design, which mitigates thermal stress and optimizes energy output. It provides a promising approach to advancing PV cooling technologies and a scalable solution for improving solar energy efficiency.

1. Introduction

Solar cell technology has advanced remarkably, increasing cost-effectiveness and efficiency while expanding its uses in numerous industries. Due to these developments, PV systems are important in the global switch to renewable energy, with a growing need to reduce reliance on non-renewable energy sources. Depending on the material's characteristics and configurations, photovoltaic cells can convert incident solar radiation into electricity, typically ranging from 10 % to 20 % efficiency [1]. The optical surface space to the receiving solar cell area is the geometric concentration ratio (CR). The ratio is usually expressed as "suns" (1sun = 1000 W/m^2 of irradiation) [2]. Photovoltaic cells exposed to elevated solar radiation concentrations experience significant temperature increases, Leading to decrease electrical efficiency of approximately 0.5 % to 0.65 % for each 1 °C rise in temperature [3]. It has been underlined that the degradation rate of the solar cell is able to twice over time for a 10-degree Celsius increase in operable temperature and then reduction in the lifespan [4]. To remedy this issue, effective cooling techniques are essential to regulate cell temperature and ensure optimal system performance. The conventional air convection heat transfer method has reached its thermal limits, necessitating the development of a more efficient cooling solution [5]. Traditionally, the heat sink has been configured to address the thermal management challenges of electronic devices [6]. However, it has since evolved to satisfy the increasing demands of photovoltaic (PV) systems cooling in solar applications [7]. Research is focused on developing novel heat sink geometries, moving beyond conventional straight-fin to more complex configurations, including fin geometry (the influence of geometrical parameters), shape, and orientation. This will improve the cooling system's fluid flow dynamics and expand the surface area for heat dissipation, enhancing heat transfer [8].

Fig. 1(a),(b),(c) which are based on the literature, explain the impact of fin optimization and their shapes in macro-size to improve solar cell performance. For instance, Johnston et al. [9] have studied the effect of fin height on heat sink efficiency in solar cells (Fig. 1(a)), revealing that

* Corresponding authors.
E-mail addresses: m.siameur@univ-batna2.dz (M. Si-Ameur), iadnan@ukm.edu.my (A. Ibrahim).

https://doi.org/10.1016/j.solener.2025.113326
Received 30 December 2024; Received in revised form 30 January 2025; Accepted 31 January 2025
Available online 16 February 2025

Nomenclature

A_c	area of solar cell (mm^2)
A_f	area of fluid domain (mm^2)
C_p	specific heat capacity (j/kg-k)
D_h	hydraulic diameter (mm)
I	solar radiation (w/m^2)
h_c	average heat transfer coefficient ($w/m^2.k$)
H	height of heat sink (mm)
H_c	height of fin (mm)
H_b	thickness base up(mm)
H_b’	thickness base-down bottom (mm)
k	thermal conductivity (w/m-k)
L	length of a heat sink (mm)
$\dot{m}$	the mass flow rate of air (g/min)
Nu	Nusselt number
ΔP	pressure drop [pa]
P_c	electrical power of solar cell (w)
Re	Reynolds number
T_c	solar cell temperature (°c)
$T_{c\ avg}$	the average cell temperature
T_{in}	the air inlet temperature
T_a	the ambient temperature
T_{out}	the air outlet temperature
T_{mean}	the average temperature of the inlet and the outlet of the air-fluid
T_w	the temperature of the fin wall
T_b	the temperature of a base heat sink
V_{in}	the inlet velocity (m/s)
W	width of a heat sink (mm)
W_c	channel width (mm)
W_W	fin width (mm)

Greek Symbols

η_c	cell electrical efficiency of solar cell
τg	the transmittance of the cover above the solar cell
η_{ref}	electrical efficiency of solar cell reference
f	the friction factor

Abbreviations

CPV	concentrator photovoltaic
Eq	Equation
HCPV	high concentrator photovoltaic
HP	heat pipe
HS	heat sink

increasing fin height (from 20 mm to 300 mm) reduces front module temperature from 62 °C to 45 °C. Similarly, Del Rïo et al. [10] have improved the electrical efficiency of solar panels by 1.07 % due to the optimum height of the heat sink to 50 mm. Furthermore, Ahmed et al. [11] have proposed a new design of a truncated multi-level fin heat sink (MLFHS), which has also been optimized for fin spacing, height, and thickness effects. The design achieves a 2.87 % rise in power output. Zaghloul et al. [12] have evaluated four heat sinks: flat plate, straight, pin, and flared (Fig. 1(b)), to enhance the temperature uniformity of triple-junction solar cell (TJ) exposed to high concentration ratios. Their findings prove that the flared-finned heat sink is an effective choice for maintaining optimal cell performance. Also, Krstic et al. [13] have

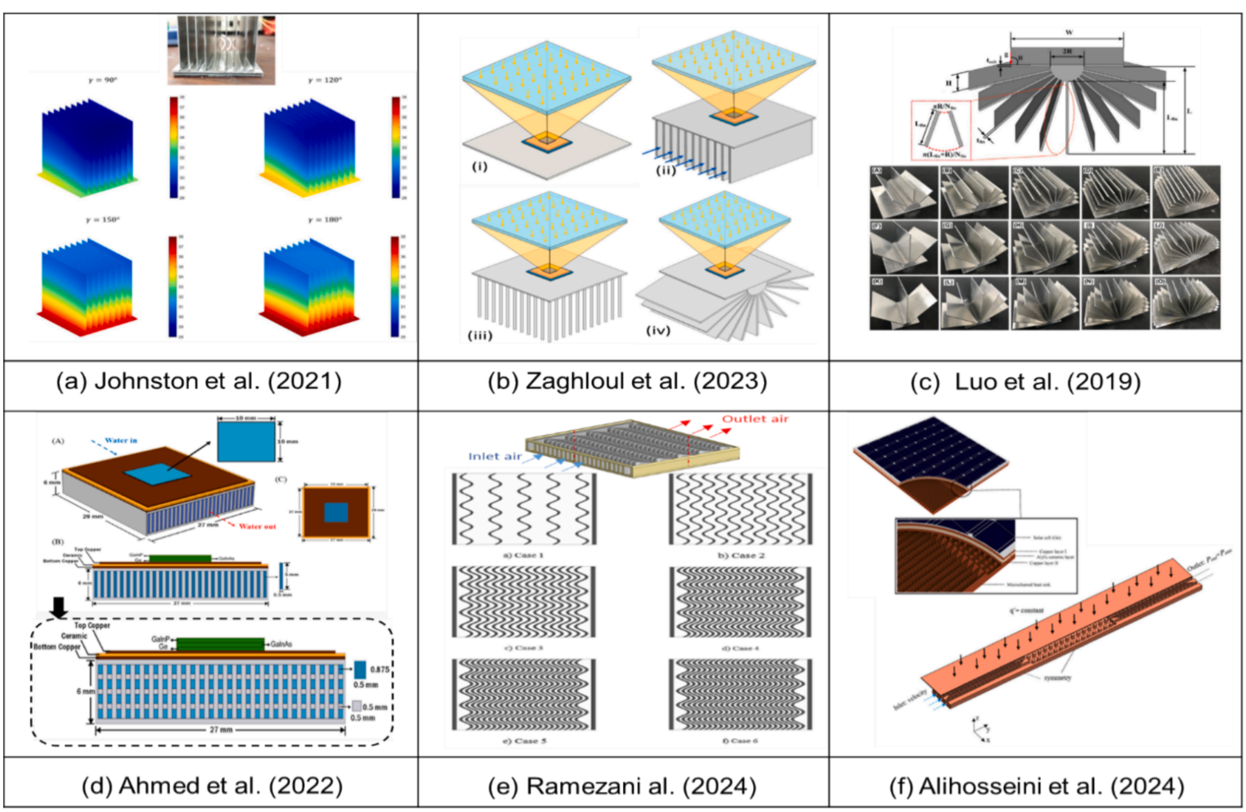

Fig. 1. (a) A rectangular finned heat sink, (b) different heat sink types: flat plate, straight, pin, and flared, (c) flared heat sink, (d) stacked and truncated single-layer mini-channel heat sink, (e) micro-channel sinusoidal fins heat sink, (f) hybrid configuration combines oblique micro-channel and micro pin fin.

reported that the passive cooling of a PV module was achieved through various shapes of heat sinks, leading to an average temperature decrease of 7.5 °C and a voltage increase of 0.27 V compared to the reference panel. They also investigated the optimal geometry for heat sinks and analyzed their heat transfer characteristics. Likewise, Luo et al. [14] have improved the cooling method with flared-fin design heat sinks for concentrator photovoltaic (CPV) systems based on the effect of adding fin number, height, and inclination angle of a fin heat sink (Fig. 1(c)). It is particularly found that the thermal resistance is reduced by 10 % compared to heat sink with rectangular fins.

The current trends of cooling employed in literature are based on mini-channel and micro-channel heat sinks, as seen in (Fig. 1(d),(e),(f)). Mini/micro channels increase the heat exchange surface area in small areas, improve the convective heat transfer coefficient, and enable integration into solar applications. The optimization scrutinizes the hydraulic diameter, cross-sectional shape, channel pattern, manifold configuration, and inlet–outlet port design, which are examples of geometric factors that can have a major impact on heat removal improvement [15,16]. Ahmed et al. [17] have employed A mini-channel heat sink utilizing nanofluids to regulate multi-junction solar cell temperatures in high concentrator photovoltaic (HCPV) systems within operational limits. Their results showed the highest thermal and electrical efficiencies were recorded at 65.40 % and 40.84 %, respectively. Similarly, Ahmed et al. [18] have examined using a finned mini-channel heat sink to limit the high temperatures found in HCPV systems. Three cooling fluids are evaluated: water, ethylene glycol, and syltherm oil 800. Their findings indicated that water exhibited the highest thermal and electrical efficiencies, with a minimum temperature of 93.5 °C. Additionally, a study by Okasha et al. [19] examined numerically truncated mini-channel heat sinks for (CPV) cooling (Fig. 1(d)), and their results revealed a 31 % rise in electrical efficiency. Torbatinezhad et al. [20] have proposed a new design of a mini-channel heat sink with zigzag fins to improve cooling efficiency compared to traditional design. Their results have found both the thermal resistance and Nusselt number are enhanced by 13 % and 12 %, respectively. Sadinezhad Fard et al. [21] have investigated the impact of the height, and base of mini-channel with grooves and ribs on the cooling efficiency of the CPV system. Compared to simple channels, they demonstrated a 25.9 % reduction in thermal resistance at the optimal height rib of 0.2 mm and a maximum temperature reduction of 6.48 K. Ramezani et al. [22] have used a microchannel heat sink with sinusoidal fins (Fig. 1(e)). They showed that the increased number of fins significantly enhanced the electrical efficiency for the solar cell (HCPV), reaching up to 38.97 % in the optimal case. Furthermore, Jatau et al. [23] have enhanced cooling efficiency in (HCPV) by utilizing a square pin–fin array in the center of a micro-channel heat sink. Their findings indicated that cell efficiency significantly improves with flow rates, and the optimal case achieves an electrical efficiency of 40.01 %, surpassing the case reference of 39.91 %. Lastly, Alihosseini et al. [24] have completed the optimal configuration, spacing, and positioning of pin fins inside the oblique grooved micro-channel heat sink (Fig. 1 (f)) to enhance cell (HCPV)performance, and their results indicating that the maximum output electrical power reached 18.443 W.

As the present investigation draws inspiration from conventional macro-scale designs, it is judicious to reference earlier studies that highlight this approach in PV cell cooling. Notably, Soliman et al. [25] demonstrated that a heat sink with forced convection could reduce cell temperature by only 11 %. In a subsequent study, Soliman et al. [26] explored two distinct cooling methods: a flat heat pipe (HP) featuring a 100 mm condenser section with a 300 mm adiabatic section coupled with a heat sink (HP Hs1) and another configuration with a 200 mm condenser and a 200 mm adiabatic region (HP Hs2). Both methods utilized forced convection cooling. The results indicated temperature reductions of approximately 28.98 °C and 31.07 °C for HP Hs1 and HP Hs2, respectively, emphasizing the limitations of these cooling systems. In the present experimental study, an innovative heat sink design significantly departs from traditional macro-sized, straight-fin heat sinks by adopting an advanced mini-channel structure. This design incorporates folded mini-channels characterized by U-shaped fins. By opening the base, the design enhances airflow distribution, improves thermal management, and creates multiple airflow pathways, facilitating more efficient heat dissipation. Narrowing the channels slows the airflow, enabling more effective heat extraction. The heat sink features 40 fins, and the increased fin density provides greater surface area for contact with the surrounding air, thereby enhancing convective heat transfer and reducing solar cell temperature. Furthermore, the lightweight nature of this design makes it particularly well-suited for applications in solar photovoltaic (PV) systems, where weight and space constraints are critical.

The proposed design will be experimentally evaluated to gather real-world performance data. Indoor experiments will be conducted under controlled conditions, including inlet air velocity rates of 0.3, 0.6, 0.8, and 1 m/s, corresponding to rates of mass flow of 120, 240, 300, and 360 g/min, and solar irradiance of 500 and 1000 W/m2. The solar cell's performance will be assessed by measuring temperature, calculating efficiency, and evaluating electrical power output. Additionally, the thermo-hydraulic performance will be determined by calculating the heat transfer coefficient, Nusselt number, and pressure drop across varying Reynolds numbers to validate the results against numerical simulations.

2. Methodology

2.1. Numerical simulation and experimental investigation

The flowchart in Fig. 2 illustrates the rigorous research process undertaken in this present investigation to numerically and experimentally evaluate a novel heat sink geometry designed to improve the cooling performance of solar cells. The first phase involved numerical simulations conducted using ANSYS FLUENT 17.1 Computational Fluid Dynamics (CFD) software. A mesh analysis was performed for each geometry by progressively reducing the grid size from 3 mm to 0.5 mm, resulting in four meshing case studies. The accuracy of the results improved with finer meshing, and an optimal model was identified, achieving a minimal relative error of 0.006 % with 6,646,412 mesh elements, thereby confirming its reliability and precision. The boundary conditions for the numerical simulations were consistent across all geometries. Both the ambient and entry air temperatures were held at 25 °C, with the inlet air velocity varying between 0.3 and 1 m/s (incremental steps of 0.1 m/s). The uniform heat flux density applied to the solar cell ranged from 500 to 1000 W/m^2. Adiabatic boundary conditions were assigned to all solid sides except for the top wall of the geometry, which was exposed to heat flux density. The outlet pressure was specified as 0 Pa, and the solar cell sides were considered adiabatic. The second phase comprised experimental validation. The optimal heat sink geometry identified during the simulation phase was fabricated and tested under controlled conditions. The experimental setup was designed to evaluate the heat sink's thermal performance and cooling efficiency, confirming it proved to be the most effective configuration among the tested models.

These complementary numerical and experimental approaches provide a robust framework for assessing and optimizing advanced heat sink designs. This methodology contributes to the development of efficient thermal management solutions for solar cells, addressing critical challenges in renewable energy systems.

2.2. The Physical model

This study evaluates the performance of two encapsulated polycrystalline solar cells sealed with polymeric materials. Table 1 presents the specifications of PV solar cells. Fig. 3 depicts the system under investigation, consisting of a solar cell attached to a heat sink.

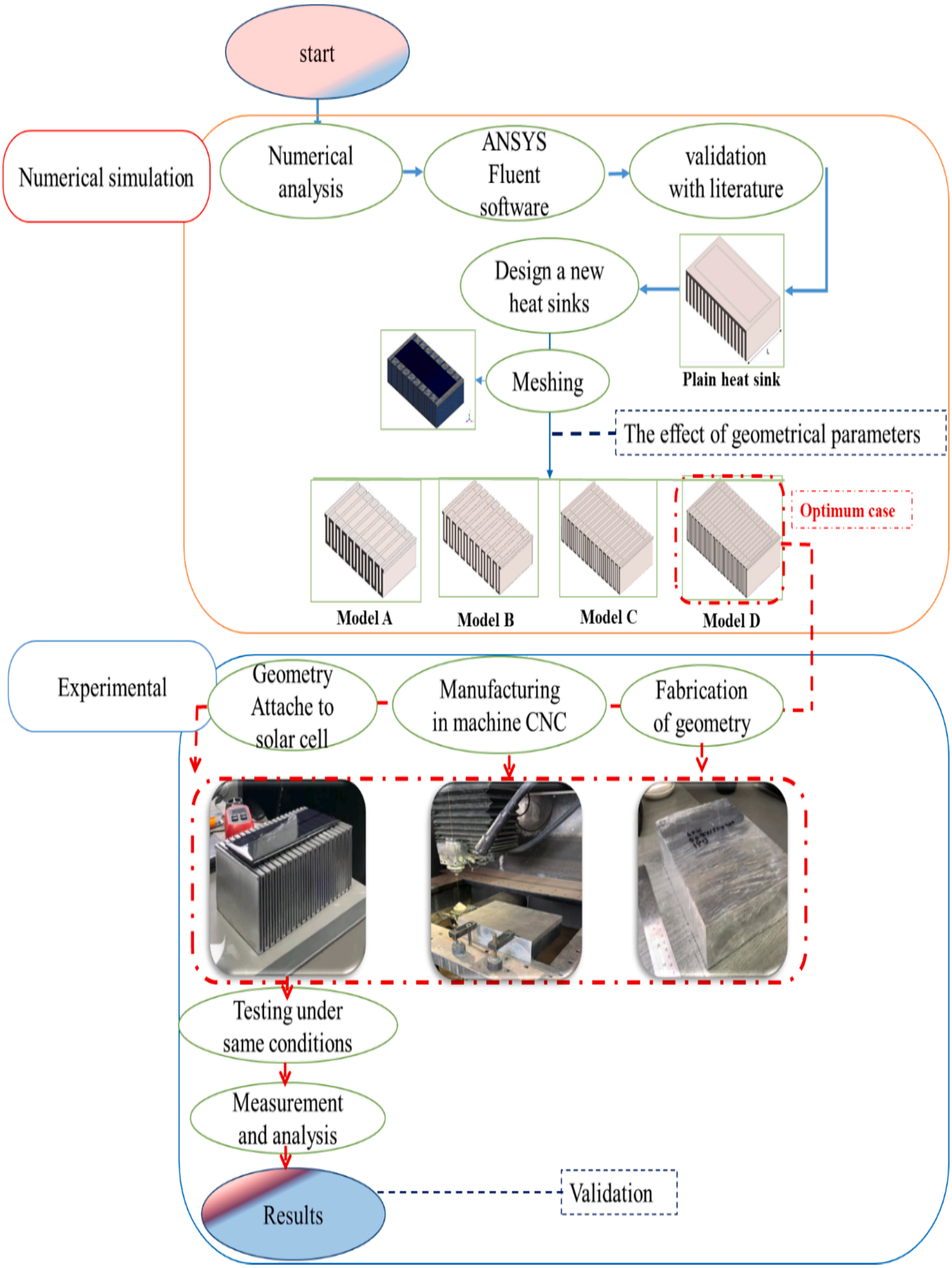

Fig. 2. Flowchart of research workflow and steps.

2.3. Design heat sink

The proposed design involves a folded mini-channel heat sink to enhance surface heat transfer, and the base of the geometry was opened to make direct contact with the solar cell. Additionally, this modification caused the fin to change into a U-shaped design with 40 fins. Air was utilized as the cooling fluid, and the design was fabricated of aluminum alloy (6061) as specified in Table 2, with dimensions according to Fig. 4 (a) and Table 3. A CNC machine cut the aluminum block, creating a new heat sink model. Conductive epoxy (ICE FUSION V2) was applied to glue

Table 1
Detailed specifications of the solar cell used in the study.

PV parameters	Description
Solar cell type	Polycrystalline
Size of the cell	165 mm*65 mm
Rated voltage	6 V
Rated current	250 mA
Peak power	1.5 W
Weight	40 g
Standard Test Conditions	1000 W/m^2,1.5AM,25 °C

the back solar cell with the heat sink base. It decreases the thermal resistance between interfaces by filling the air gaps. It has a thermal conductivity of 5 (W/m-K), as shown in Fig. 4 (b). Lastly, thermocouples were placed at three locations to test the fins and base heat sink.

2.4. Experimental setup

The indoor experiment was conducted in the Solar Thermal and Sustainable Technology lab at SERI, Universiti Kebangsaan Malaysia (UKM). The experiment setup followed a methodology based on prior literature [25,26]. The initial experiment involved testing the solar cell without a cooling system to establish a performance baseline, as shown in Fig.5 (a). The infrared camera (Fluke TiR32) recorded the temperature distribution throughout the solar cell area, as shown in Fig. 5 (b); subsequently, the data was transferred to The FLUKE Connect software on a laptop. Additionally, as shown in Fig. 5 (c) and (d), the attached heat sink was used to test and assess the effectiveness of the proposed novel folded mini-channel heat sink system for cooling a solar cell. A solar simulator used in the study has 8 tungsten halogen lamps, each having a maximum output of 300 W, thermocouples type K connected to a data logger (At4824 Digital Temperature Data Recorder Display 24 Channels) using 12 thermocouples. Table 4 shows the distribution of them placed around the test setup. All thermocouples must have their values equal to the ambient temperature before running the experiment. The air conditioner maintains a constant ambient temperature of 25 °C. A fan (12 V DC) is an active part of the system that operates by forced airflow toward the fins. The mini digital anemometer (UNI-T UT363) measures air velocity variation, and the manometer (UNI-T UT366A) measures pressure. It is located close to the heat sink's inlet. Then, the experiment is conducted using inlet air velocity of 0.3, 0.6, 0.8, and 1 m/s, as well as solar irradiances of 500 and 1000 W/m^2, respectively. The halogen lamps generate solar irradiation, which we quantify using a pyranometer or solar power meter (RS PRO ISM400). Lastly, before repeating the same procedure for the next solar irradiance levels, the system ought to cool down for an hour.

3. Background and relevant equations

3.1. Cell temperature and electrical performance

The average cell temperature (Tc_{avg}) is obtained using Eq.1:

$$T_{cavg} = \frac{\sum T_c}{N} \quad (1)$$

Tc denotes the instantaneous cell temperature recorded at various intervals, while N signifies the total number of readings obtained.

The solar cell efficiency as influenced by the cell temperature in Eq.2 of Evans and Florschuetz formula [27]:

$$\eta_c = \eta_{ref}\left[1 - \beta_{ref}\left(T_{cavg} - T_{ref}\right)\right] \quad (2)$$

β_{ref} refers to the solar cell's relative temperature coefficient of 0.004 °C^{-1} in the reference temperature of $T_{ref} = 25$ °C.

Calculating the produced electrical energy is as follows using Eq. (3) [27]:

$$P_c = \eta_c \times \tau g \times I \times Ac \quad (3)$$

Table 2
Thermal system materials properties detail.

Material	Property	symbol	Value	unit
Air at (25c°)	Density	(ρ_{air})	1.184	[kg/m^3]
	Kinematic viscosity	(ν_{air})	1.849.10^{-5}	[m^2/s]
	Thermal conductivity	(k_{air})	0.02551	[W/m.K]
	Specific heat	($C_{p\ air}$)	1007	[J/kg.K]
Aluminum	Density	(ρ_{al})	2719	[kg/m^3]
	Thermal conductivity	(k_{al})	202.4	[W/m.K]
	Specific heat	($C_{p\ al}$)	871	[J/kg.K]

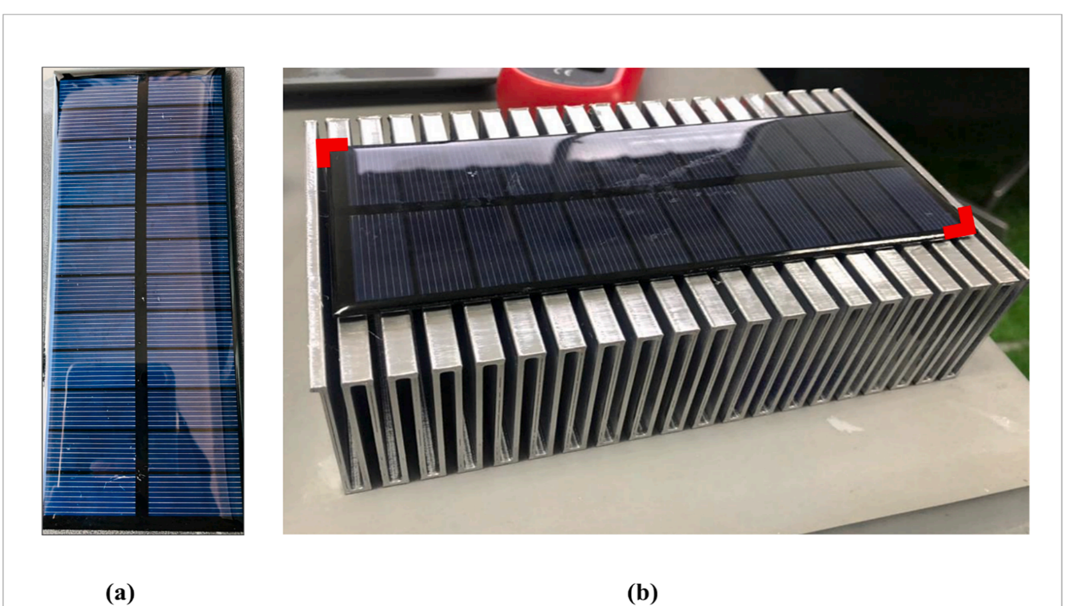

Fig. 3. (a) Reference solar cell, (b) An innovative design featuring a folded mini-channel heat sink attached to a solar cell.

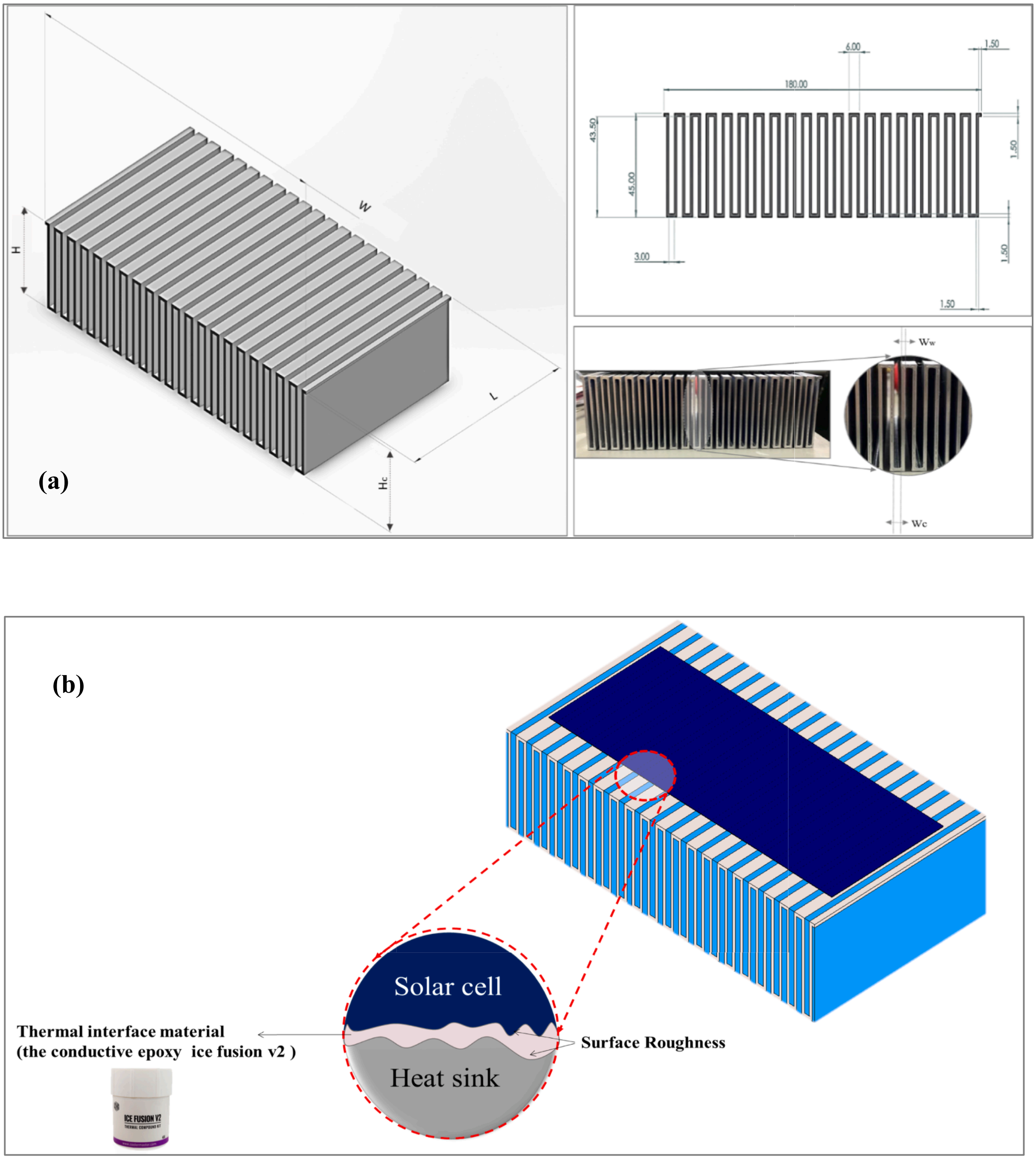

Fig. 4. (a) 3D and 2D views of the folded mini-channel heat sink with main dimensions, (b) schematic vision of the surface roughness interface.

Table 3
Geometrical characteristics and dimensions of the heat sink.

Parameters	Symbol	Value	Unit
Width heat sink	W	180	mm
Length heat sink	L	100	mm
Height heat sink	H	45	mm
Thickness base-up	H_b	1.5	mm
Thickness base-down	H_b'	1.5	mm
Wall width fin	W_w	1.5	mm
Height channel	H_c	43.5	mm
Width channel	W_c	3	mm
Hydraulic diameter	D_h	5.61	mm
Number of fins	N_f	40	–

3.2. *Themofluide data processing*

The present study investigates the heat transfer rates of internal cooling wall fins, considering a wide range of air inlet velocity, a new version of the heat sink's geometric dimensions, and the input of heat density. The Reynolds number is determined using the hydraulic diameter, as Eqs. (4)–(5).

$$\mathrm{Re} = \frac{\mathrm{V_{in}\,D_h}}{\nu_{air}} \tag{4}$$

$$\mathrm{D_h} = \frac{4(\mathrm{H_c W_c})}{2(\mathrm{H_c} + \mathrm{H_c})} \tag{5}$$

The average heat transfer convection coefficient is determined by

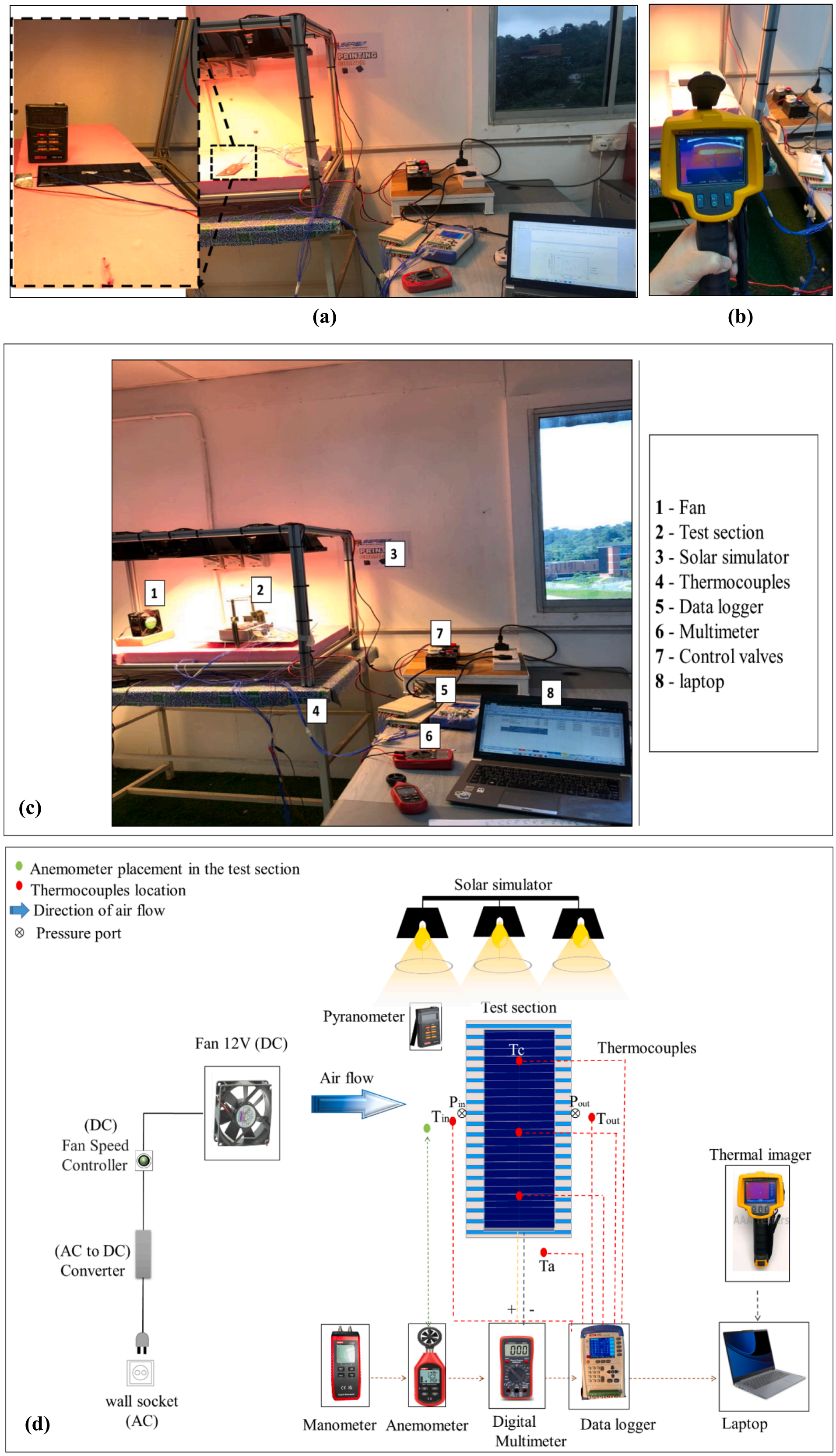

Fig. 5. (a) Real photograph of test solar cell without cooling, (b) thermal camera used in the test, (c) real photograph of the experimental system indoors, (d) schematic vision diagram of the experimental setup.

Table 4
Distribution of thermocouples on the test rig.

Channel in Data logger	Location
C1,C2,C3	T_w
C4,C5,C6	T_b
C7	T_{in}
C8	T_{out}
C10	T_a
C11,C14,C15	T_c

Newton's law Eqs. (6)–(7) [28]:

$$h_c = \frac{Q_w}{A_f(T_w - T_{mean})} \tag{6}$$

$$T_{mean} = \frac{T_{in} + T_{out}}{2} \tag{7}$$

T_w is the fins wall temperature, and T_{mean} is the average temperature between the inlet and the outlet of the airflow. Heat energy in Eq. (8):

$$Q_w = \dot{m}.cp.\ (T_{out} - T_{in}) \tag{8}$$

The average Nusselt number is calculated using Eq. (9):

$$Nu = \frac{h_c D_h}{k_{air}} \tag{9}$$

The following correlation provide the friction factor of laminar flow at Reynolds numbers below 600 by Jiang et al. [2930]:

$$f = 1639/Re^{1.48} \tag{10}$$

Pressure drop is calculated using Eq.11 [30]:

$$\Delta p = f \times \frac{L}{D_h} \times \frac{\rho V_{in}{}^2}{2} \tag{11}$$

Where L is the length of a mini-channel heat sink.

Improvement of cooling.

A comparative study on the reduction in solar cell temperature and the improvement in electrical power output performance was conducted using Eq. (12) to calculate the percentage difference [31]:

$$\%Tc = \frac{Tc\,ref - Tc\,cooling}{Tc\,ref} \times 100 \tag{12}$$

Eq.13 is used to calculate the percentage error between numerical simulations and experimental results.

$$\%E = \frac{Rsim - R\exp}{R\exp} x\,100 \tag{13}$$

3.3. Uncertainty analysis

Errors can arise from humans, tools, and devices. Assessing sensor uncertainty and determining in-reading errors is crucial for high-quality measurements. The following (Eq. (14) and Table 5 served as the basis for the uncertainty analysis of the experimental test instruments [32,33]:

Table 5
Error range for each instrument employed in the study.

Equipment	Model	Parameters	Unit	Uncertainty (%)
Data Logger	AT4824	Temperature	oC	±0.1
Thermocouples	K-type	Temperature	oC	±0.1
Pyranometer	RS pro-ISM 400	Solar irradiance	W/m²	±1
Manometer	UNI-T UT366A	Pressure	Pa	±0.5
Anemometer	UNI-T UT363	Air velocity	m/s	±0.1
Thermal imager	Fluke TiR32 Infrared Camera	Temperature	oC	±2

$$W_R = \left[\left(\frac{\partial R}{\partial X_1}W_1\right)^2 + \left(\frac{\partial R}{\partial X_2}W_2\right)^2 + \cdots\cdots\left(\frac{\partial R}{\partial X_n}W_n\right)^2\right]^{\frac{1}{2}} \tag{14}$$

$$W = \left[(0.1)^2 + (0.1)^2 + (1)^2 + (0.1)^2 + (0.5)^2 + (2)^2\right]^{\frac{1}{2}}$$

$$W = 2.29\%$$

4. Results and Discussion

4.1. Cell temperature

Fig. 6 illustrate the solar cell front-surface temperature variation over a 25 min monitoring period. The influence of inlet air velocity on the thermal performance of the solar cell system is evident for the two target solar irradiance 500 and 1000 W/m^2.

Fig. 6 (a) compares two cases of solar cell operation. Without cooling, the initial temperature of the cell starts at 38 °C due to prior exposure to light before the measurement, indicating that the cell had already absorbed heat. The temperature rises rapidly during the test, reaching approximately 68 °C under a solar irradiance of 500 W/m^2. This demonstrates the necessity of cooling to prevent overheating. In contrast, the optimum cooling case, using forced convection at an inlet velocity of Vin = 1 m/s, maintains a low and stable cell temperature, as shown by the cooling curve.Fig. 6 (b) examines the impact of different inlet velocities on cell performance. As inlet velocity increases, cell temperature decreases. At lower velocities Vin = 0.3 m/s, the temperature gradually rises to 36 °C over time. Conversely, at higher velocities (Vin = 0.8 and Vin = 1 m/s), the cell temperature stabilizes after a few minutes, indicating that equilibrium is achieved, where heat dissipation matches heat generation.

Fig. 7 illustrates the thermal response of the system across all inlet velocities. During the first 5–10 min, the temperature increases significantly as the system transitions from ambient temperature to a heated state. After approximately 15 min, the temperature stabilizes, indicating that the system reaches a steady state. At lower velocities, the cell temperature stabilizes at 43 °C and 41 °C, respectively, highlighting the limited cooling effect of natural convection at high solar irradiance (1000 W/m2). At higher velocities (Vin = 0.8 m/s and Vin = 1 m/s), the temperature of the cell drops to 38 °C, showcasing the effectiveness of forced convection.

Fig. 8(a) shows the average cell temperature, calculated using Eq. (1), under irradiance levels of 500 and 1000 W/m2. It is shown that. Without cooling, the solar cell temperature ranges between 67 °C and 86 °C, demonstrating that increased irradiance intensity results in higher temperatures and necessitates more efficient cooling. With the application of a heat sink and varying inlet velocities (Vin = 0.3,0.6,0.8, and 1 m/s), the recorded cell temperatures under 500 W/m2 irradiance are 34.35 °C, 33.57 °C, 32.55 °C, and 31.13 °C, respectively. Similarly, under 1000 W/m2, the cell temperature decrease to 40.44 °C, 38.93 °C, 37.94 °C, and 36.99 °C. The percentage curves based on Eq. (9), which illustrate the improvement in cooling At V_{in} = 1 m/s, show a maximum reduction temperature of 57.47 % at higher irradiance intensity. Even at 500 W/m2, it maintained at 53.86 %The U-shaped folded mini-channel design decreased the solar cell's temperature by 57.44 %. In comparison, as reported in the literature [34], conventional finned container heat sink, lower the operating temperature of photovoltaic panels by 10.53 %, from 57.9 °C to 51.8 °C. This trend in dropping temperature in higher solar irradiance indicates high capabilities of the folded heat sink to remove furthere heat and enhancing its thermal performance.

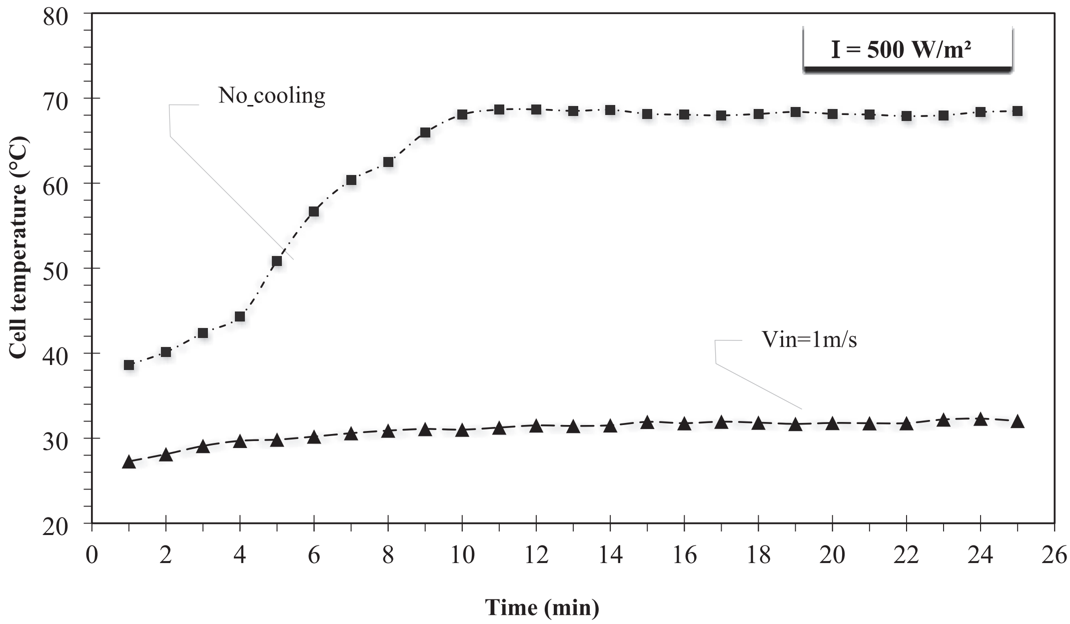

(a)

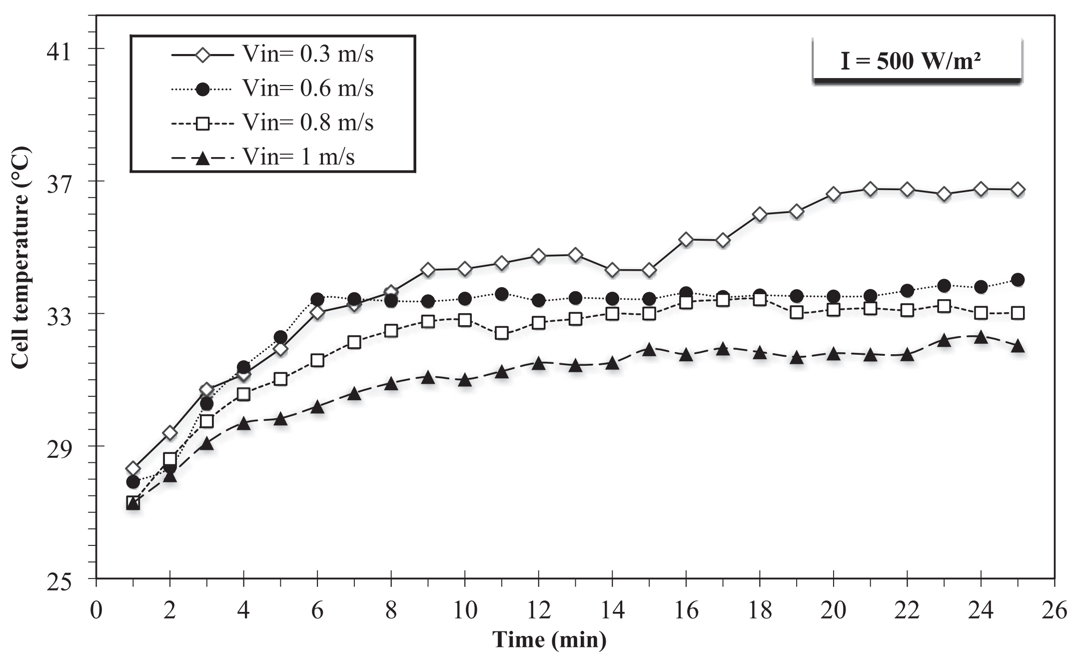

(b)

Fig. 6. (a) Solar cell temperature varitaion over time with and without cooling, (b) Solar cell temperature over time at a solar irradiance level of 500 W/m^2 and different inlet air velocity.

4.2. Electrical cell efficiency

In Fig. 8 (b), the cell electrical efficiency throughout the experiment is calculated using Eq. (2) versus the inlet air velocity rates. The cooling system's effectiveness is evaluated by observing the improvement in the electrical efficiency between two solar cells (no cooling/cooling) under varying irradiance intensities. The results indicate that in lower irradiance of 500 W/m2, the new cooling model mini-channel heat sink significantly enhances PV cell efficiency from 12.45 % to 14.63 % for recorded via increased inlet velocity; the improvement increased in difference to 1.99 %, 2.03 %, 2.10 %, and 2.18 %, respectively. Even under high-intensity irradiance 1000 W/m2, the diminished efficiency compared to lower irradiance increased from no cooling from 11.28 % to 14.28 % cooling recorded via increased inlet air velocity; the improvement increased 2.79 %, 2.88 %, 2.94 %, and 3.00 %, respectively. Comparison with literature reviews [34] indicates that a finned container heat sink improved the module efficiency by 5.3 %, corresponding from 9.33 % to 9.82 %. This can be due to the substantial temperature increase of the PV cell, which impairs their performance. Overall results are evidence this novel model offers a feasible pathway to enhance the electrical efficiency of photovoltaic cells.

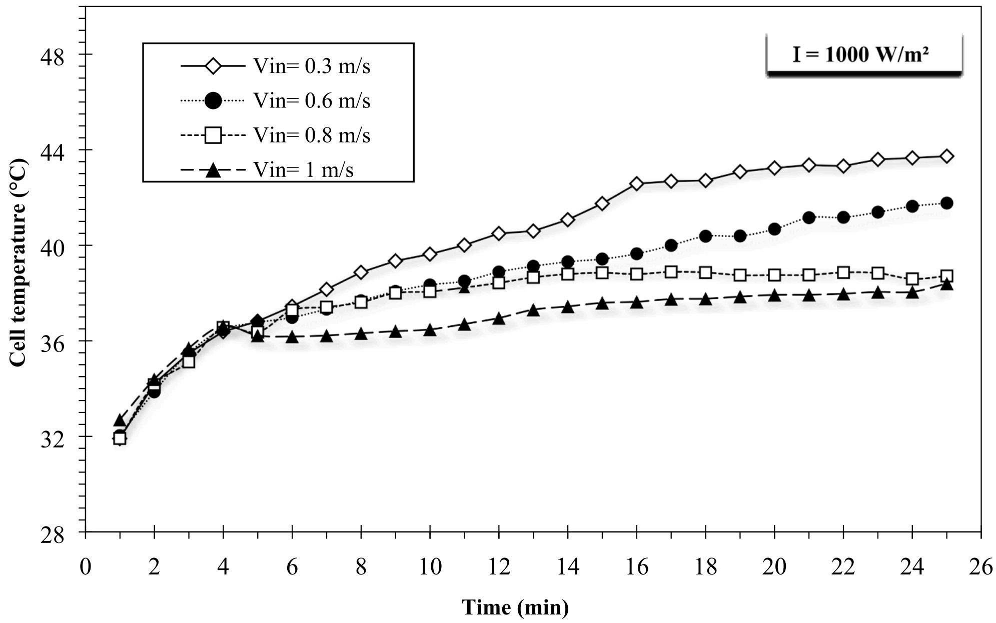

Fig. 7. Solar cell temperature over time under solar irradiance 1000 W/m^2 and different inlet air velocity.

4.3. Electrical cell power

Fig. 8(c) illustrates the electrical output power generated by two solar cells versus the inlet air velocity under varying irradiance intensities (500, 1000 W/m2). The Eq. (3) was employed to calculate the power output. Based on findings, the integration of folded mini-channel heat sink to solar cell evidence due to increased electrical power difference between (no cooling /cooling) 0.098 W,0.162 W,0.165 W, and 0.170 W respectively recorded via increase inlet air velocity under 500 W/m2. In contrast, increments are more pronounced in I = 1000 W/m2 by 0.275 W, 0.405 W, 0.412 W, and 0.418 W. So, the solar cell's efficiency has been enhanced as a result of larger temperature reduction achieved by cooling at 1000w/m2, which has resulted in a more significant increase in electrical power. Lastly, data provided confirm that a new heat sink significantly outperforms by a reduction in temperature, increasing the electricity efficiency and power.

Fig. 9 displays an infrared thermal image for two solar cells showing a graphical representation for the temperature distribution across the surface with no cooling and a cooling system in 500 W/m^2 solar irradiance. This is intended to serve as additional backup information to the thermocouple results that were previously obtained, as previously described. Fig. 9 (a) illustrates a uniform distribution of high temperatures across the majority of the surface, with the addition of three randomly placed points on the left, middle, and right, respectively, to determine the hottest zone within the surface cell. The results show the hottest point P2 is 69.53 °C at the left edge of the surface, and the P1 and P3 center of the surface and the right edge show lower values of 66.42 °C and 65.52 °C respectively. The heat accumulates on the left edge because the solar simulator emits uniform irradiation. Still, some zones may receive less radiation in the test area, which is evident. Fig. 9 (b) shows the effect of integrating design to cooling a cell as the temperature decreases; the cooler regions at the periphery are P3 at 31.80 °C and P1 at 32.28 °C. The hotspot in the left zone P2 at 33.41 °C, is a reason for the airflow's inability to reach all fins uniformly. Effectively, the cooling system has an advantageous impact.

4.4. Outlet temperature

Fig. 10 represents outlet air temperature and the temperature differences versus inlet mass flow rate under solar irradiance. With lower inlet mass flow rates of 120 g/min to 200 g/min, the outlet air temperature is higher, reaching 29.24 °C and 28.12 °C at W/m^2. This indicates the air stays in the fins of heat sink longer, enabling it to absorb additional heat, leading to a higher outlet temperature. Consequently, the inlet and outlet air temperature difference is also more significant, indicating more efficient heat extraction from the heat sink to the air. At higher 500 W/m^{2}and 30.20°Cand 29 °C at 1000 mass flow rates of 300 g/min and 360 g/min, the outlet air temperature decreases to 27.29 °C and 27.13 °C for 500 W/m^2 and 28.26 °C and 28.08 °C for 1000 W/m^2. The smaller residence time of air leads to a reduction in heat absorption, which results in cooler outlet air temperatures, leading to smaller temperature differences. Outlet air temperatures are significantly affected by solar irradiances: at 1000 W/m^2, the outlet air temperature is consistently higher than 500 W/m^2. The reason is that intensity introduces more heat into the system, increasing the temperature of the air passing through a heat sink.

5. Comparison between experimental and numerical simulations

5.1. Thermos-hydraulic parameters

Fig. 11 highlights the significant improvement in thermo-hydraulic parameters by comparing the findings with previous data simulations. Achieving an optimal balance between pressure drop and heat transfer enhancement is crucial for efficient cooling system performance. The pressure drop represents the resistance undergone the fluid as it flows through the heat sink with a positive correlation between the Reynolds number and pressure drop. This study presents three datasets for the pressure drop: measured, simulated, and calculated (via the correlation by Jiang et al. [29]), as shown in Fig. 11(a). Experimental findings reveal that the pressure drop increases progressively from 0.92 Pa, 1.8 Pa, 2.45 Pa, to 3.08 Pa, corresponding to Reynolds numbers 107.8, 215.60, 287.47, and 359.34. The numerical simulation results similarly demonstrate a consistent rise in pressure drop with increasing Reynolds numbers, reflecting higher flow resistance at greater velocities. Importantly, the increase in pressure drop remains within acceptable limits. A maximum gap of 11 % between the experimental and simulated data confirms the accuracy and reliability of both methods. The calculated pressure drop using the friction factor correlation (Eq. (10) by Jiang et al. [29] shows occasional deviations from the experimental curve. These discrepancies suggest that the correlation may not fully capture

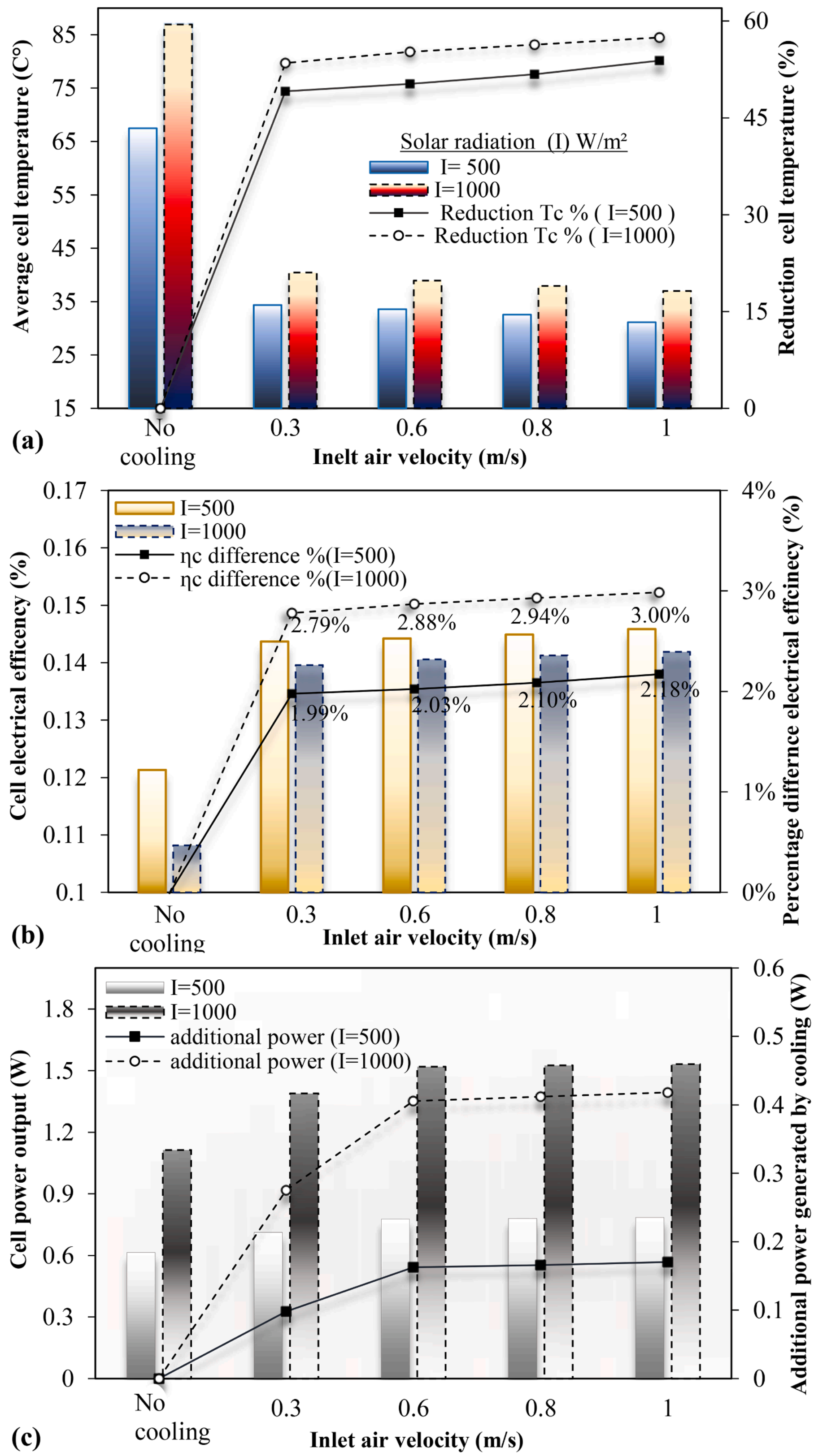

Fig. 8. (a) Average solar cell temperature and percentage reduction versus inlet air velocity. (b) electrical efficiency and improvement in electrical efficiency versus inlet air velocity. (c) electrical power and cooling gain power for various inlet air velocities and solar irradiances.

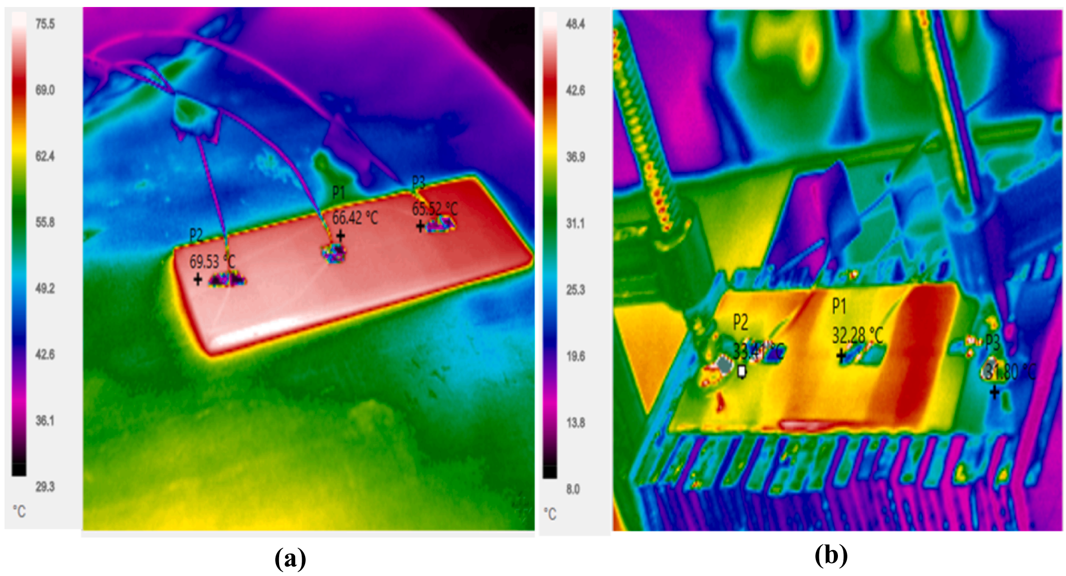

Fig. 9. Thermal image of a solar cell during operation for I = 500 W/m^2 : (a) without cooling, (b) with cooling.

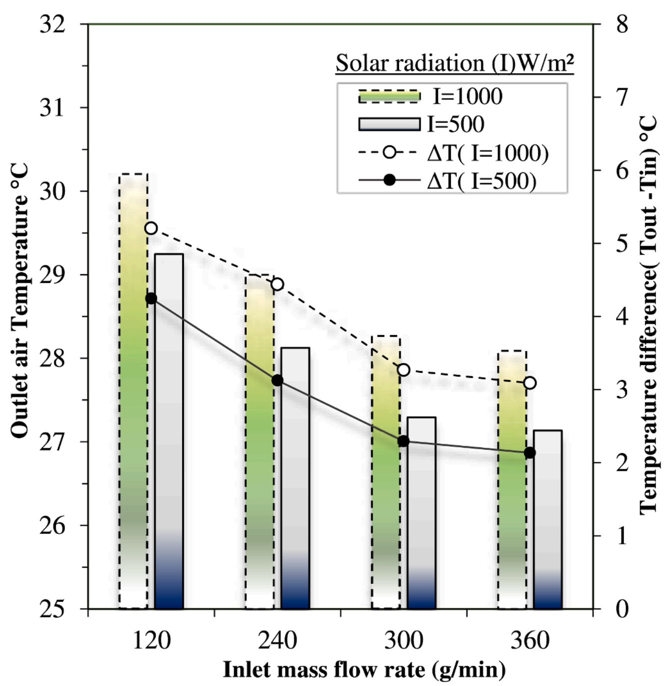

Fig. 10. Outlet air temperature and temperature differences at various mass flow rates for two solar irradiances.

the geometric complexities of the heat sink design.. As indicated, the pressure drop tends to increase with more intricate designs, such as those incorporating narrow channels or mini-channels [35].

Both numerical simulations and experimental studies consistently record the average heat transfer coefficient. Fig. 11(b) and (c) depict the average heat transfer coefficient depending of the Reynolds number under solar irradiances of 500 W/m^2 and 1000 W/m^2, respectively. Under solar irradiance of 500 W/m^2 in Fig. 11(b), simulation results show a steady increase in the average heat transfer coefficient as the Reynolds number rises. The coefficient improves from 13.49 W/m^2-K at a Reynolds number of 107 to 33.68 W/m^2-K, demonstrating better convective heat transfer at Reynolds number of 359. The experimental results follow a similar trend, ranging from 17.39 W/m^2-K a to 34.93 W/m^2-K at Reynolds number of 107 to 359 respectively. At solar irradiance of 1000 W/m^2 in Fig. 11(c), a similar pattern is observed. The numerical simulations reveal that the average heat transfer coefficient increases steadily from 12.91 W/m^2-K at a Reynolds number of 107 to 33.68 W/m^2-K at 359. Experimental results align closely, ranging from 17.67 W/m^2-K to 35.51 W/m^2-K. The increase in heat flux under higher irradiance enhances the temperature gradient between the air and the surface, thereby boosting the average heat transfer coefficient [16]. The results validate the consistency between numerical simulation and experimental data, with discrepancies within an acceptable gap margin. For the remaining three values under solar irradiance of 500 W/m^2, the error percentage is below 3 %, further emphasizing the strong agreement between the two approaches.

According to the study, determining the Nusselt number is necessary to assess the efficiency of a heat transfer process. The findings indicate a positive relation between the Reynolds and Nusselt numbers, which is in line with previous research [36]. Fig. 11 (d) and (e) present the average Nusselt number as a function of the Reynolds number for both simulation and experimental results under solar irradiation levels of 500 W/m^2 and 1000 W/m^2. Experimentally, at I = 1000 W/m^2, the average Nusselt number increases with the Reynolds number, showing values of 3.88, 5.33, 6.70, and 7.81. In comparison, at I = 500 W/m^2, the corresponding values are 3.88, 5.33, 6.50, and 7.68. These results indicate that as the flow develops at higher Reynolds numbers, enhanced convective heat transfer leads to higher Nusselt numbers. The numerical simulations consistently demonstrate the ability to predict the average heat transfer coefficient and Nusselt number accurately across all charts (a), (b), (c), and (d). Using Eq. (13) to calculate the error, the numerical simulation results show excellent agreement with experimental results. For most data points, the error percentage remains below 5 %, which is within the acceptable range, particularly at I = 1000 W/m^2. However, the initial value exhibits a maximum deviation of approximately 22 %, attributed primarily to measurement errors associated with the thermocouples. These errors directly influence the computation for both the heat transfer coefficient and the Nusselt number.

Table 6 provides a summary comparing the temperature differences (with and without cooling) obtained in this study to various other published experimental works. It highlights the impact of shaped fin heat sinks on cooling photovoltaic (PV) cells under identical solar irradiance conditions, utilizing different convection flow methods (forced or natural). The temperature reduction achieved in this present study is markedly higher than those reported in the cited literature,

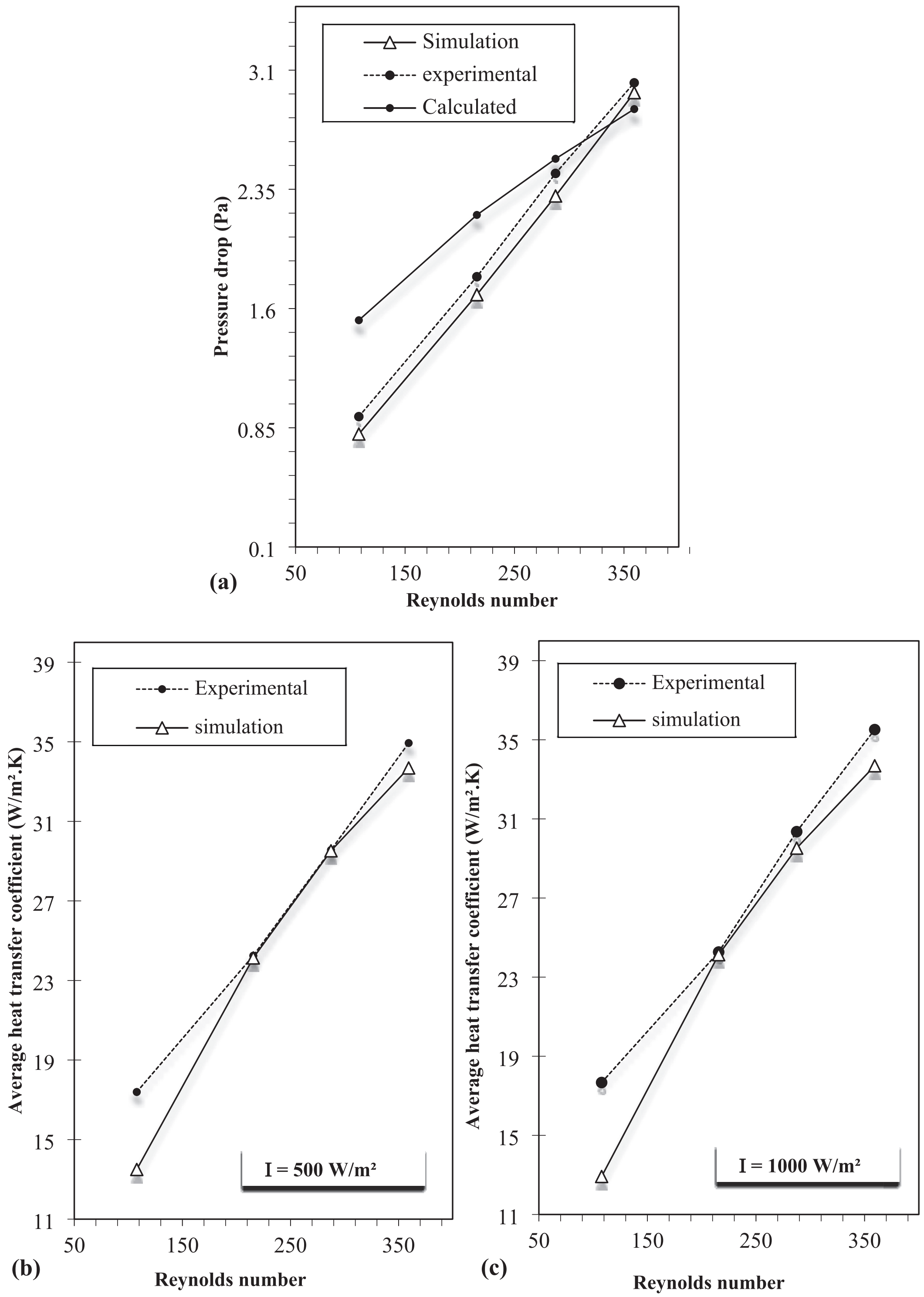

Fig. 11. Experimental and numerical simulation comparison: (a) pressure drop versus Reynolds number for three data sets: measured, simulated, and correlation; (b, c) average heat transfer coefficient versus Reynolds number for two solar irradiances; and (d, e) average Nusselt number vs. Reynolds number for two solar irradiance levels.

demonstrating the superior effectiveness of the proposed heat sink geometry for cooling. These results underscore the significant influence of the innovative heat sink design on improving thermal control in PV cells, as validated through simulations.

6. Conclusion

This experimental study examined the integration of an innovative folded mini-channel heat sink featuring small flow passages to enhance the cooling and electrical efficiency of photovoltaic (PV) cells. The results provide valuable insights into the thermal and electrical

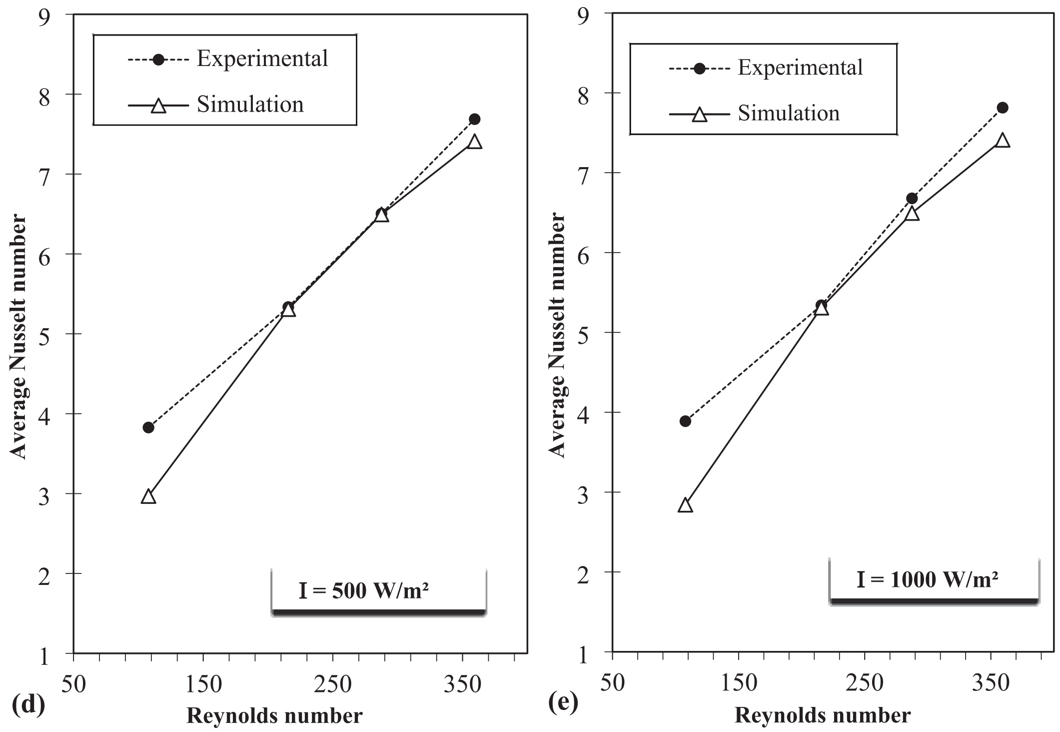

Fig. 11. (*continued*).

Table 6
A comparison of the current results with similar previous published studies.

Authors (Ref.)	Years	Study	Convection Flow	Cooling methodology	Difference temperature (°C)
Cuce et al. [37]	(2011)	Experimental	Natural	Rectangular heat sink	17.5 °C
Soliman et al. [25]	(2019)	Experimental	Natural /Forced	Rectangular heat sink	31.1 °C
Soliman et al. [26]	(2020)	Experimental	Natural /forced	A flat heat pipe with a rectangular heat sink	28.98 °C
Elbreki et al.[38]	(2020)	Experimental	Natural	Lapping fins heat sink	24.57 °C
Gomaa et al [39]	(2020)	Experimental	Natural	U shape fins heat sink	2 °C
Sivashankar et al. [40]	(2022)	Experimental	Forced	Various heat sinks shaped with PCM	up to 13 °C
Ahmed et al. [11]	(2022)	Experimental	Natural	Truncated multi-level fin heat sink (MLFHS)	up to 8.45 °C
Razali et al. [41]	(2023)	Experimental	Natural	Multidirectional Tapered Fin Heat Sink (MTFHS)	12 °C
Current study		Experimental	Forced	Folded Mini-channel Heat sink	36 °C

performance of PV cells and the thermo-hydraulic behavior of the heat sink under varying operating conditions, including different solar irradiance intensities and airflow rates. The agreement between the experimental findings and numerical simulations demonstrates reliability, with an average heat transfer coefficient error percentage below 5 %, well within acceptable limits. The key results for the study are as follows:

- The average cell temperature decreased significantly from 86.93 °C to 36.99 °C, corresponding to a 57.43 % reduction at a solar irradiance of 1000 W/m^2 and an inlet air velocity for 1 m/s.
- This temperature reduction directly improved electrical efficiency, which increased from 11.28 % to 14.28 %.
- A substantial increase in the electrical power output of the solar cell was observed, particularly under higher irradiance conditions, with a net power gain of 0.418 W.
- At an inlet air velocity of 1 m/s, the inlet and outlet air temperature difference was reduced to 3.08 °C. Despite the shorter air residence time within the heat sink, the cooling system effectively maintained the cell temperature within safe operating limits.
- These findings underline the potential of folded mini-channel heat sinks to optimize thermal management and electrical performance in PV cells, particularly in high irradiance environments.

These findings underline the potential of folded mini-channel heat sinks to optimize thermal management and electrical performance in PV cells, particularly in high irradiance environments.

- Future research should focus on outdoor experiments using natural airflow instead of fans to address inadequate airflow distribution. Additionally, updating the same model heat sink and changing from U-shaped fins longitudinal to pin fins will further enhance thermal performance.
- This innovative cooling approach could be adapted to concentrated photovoltaic (CPV) systems, which typically operate at higher temperatures due to increased solar concentration. By applying the proposed design to CPV systems, it may be possible to enhance their thermal regulation and energy efficiency, extending their applicability to regions with extreme climatic conditions.

CRediT authorship contribution statement

Amel Djebara: Writing – original draft, Methodology, Formal analysis, Conceptualization. **Nabil Bessanane:** Supervision, Methodology, Conceptualization. **Mohamed Si-Ameur:** Writing – review & editing, Methodology, Formal analysis, Conceptualization. **Adnan Ibrahim:** Writing – review & editing, Supervision, Methodology, Funding acquisition. **Zouheyr Noui:** Validation, Formal analysis. **Sharul Sham Dol:** Writing – review & editing, Supervision, Funding acquisition. **Hariam Luqman Azeez:** Validation, Formal analysis. **Sidi Ali Amira:** Validation, Formal analysis.

Declaration of competing interest

The authors declare that they have no known competing financial interests or personal relationships that could have appeared to influence the work reported in this paper.

Acknowledgement

Faithfully thank the Solar Thermal and Sustainable Technology Group, at Sustainable Resources, Nature and Smart Living Cluster, Kumpulan Penyelidikan Universiti (KPU) and Institut Penyelidikan Tenaga Suria, Universiti Kebangsaan Malaysia, For their continuous support and insightful advice throughout this research.

References

[1] S.A. Zubeer, O.M. Ali, Experimental and numerical study of low concentration and water-cooling effect on PV module performance, Case Stud. Therm. Eng. 34 (2022) 102007, https://doi.org/10.1016/j.csite.2022.102007.
[2] S.S. Indira, C.A. Vaithilingam, K.K. Chong, R. Saidur, M. Faizal, S. Abubakar, S. Paiman, A review on various configurations of hybrid concentrator photovoltaic and thermoelectric generator system, Sol. Energy 201 (2020) 122–148, https://doi.org/10.1016/j.solener.2020.02.090.
[3] A. Gupta, S.S. Chougule, S.K. Saha, Cooling of highly concentrated photovoltaic cells with confined jet impingement by introducing channel configurations, Renew. Energy 237 (2024) 121600, https://doi.org/10.1016/j.renene.2024.121600.
[4] M.S. Sheik, P. Kakati, D. Dandotiya, U.r. m, r.c. s,, A comprehensive review on various cooling techniques to decrease an operating temperature of solar photovoltaic panels, Energy Nexus 8 (2022) 100161, https://doi.org/10.1016/j.nexus.2022.100161.
[5] M.H. Elnaggar, Heat transfer enhancement by heat sink fin arrangement in electronic cooling, Heat Transfer 2 (3) (2015).
[6] J. Li, L. Yang, Recent development of heat sink and related design methods, Energies 16 (20) (2023) 7133, https://doi.org/10.3390/en16207133.
[7] G. Cătălin, V. Popovici, S. Hudişteanu, T. Mateescu, N.-C. Chereches̨, Efficiency improvement of photovoltaic panels by using air-cooled heat sinks, Energy Procedia 85 (2015) 425–432, https://doi.org/10.1016/j.egypro.2015.12.223.
[8] N. Hamza, H.K. Mohsen, Investigation of laminar forced convection using a different shape of a heat sink, Al-Qadisiyah, J Eng. Sci. 15 (2) (2022). https://doi.org/10.30772/qjes.v15i2.816.
[9] E. Johnston, P.S. Szabo, N.S. Bennett, Cooling silicon photovoltaic cells using finned heat sinks and the effect of inclination angle, Therm. Sci. Eng. Prog. 23 (2021) 100902, https://doi.org/10.1016/j.tsep.2021.100902.
[10] J.A.S. Del Rio, Y.R. Ardila, A.R. Sánchez, E.C. Quintana, D. Sanin-Villa, C. Arrieta González, M. Luna-Del Risco, Numerical study of the efficiency of a solar panel with heat sinks, CFD Lett. 15 (4) (2023) 43–52. https://doi.org/10.37934/cfdl.15.4.4352.
[11] E. Ahmad, A. Fazlizan, H. Jarimi, K. Sopian, A. Ibrahim, Enhanced heat dissipation of truncated multi-level fin heat sink (MLFHS) in case of natural convection for photovoltaic cooling, Case Stud. Therm. Eng. 28 (2021) 101578, https://doi.org/10.1016/j.csite.2021.101578.
[12] H. Zaghloul, M. Abdelrahman, M. Abd Rabbo, M. Emam, Passive thermal control of a triple-junction solar cell at high concentrations using various finned heat sink configurations, J. Clean. Prod. 387 (2023) 135844, https://doi.org/10.1016/j.jclepro.2023.135844.
[13] M. Krstic, L. Pantic, S. Djordjevic, I. Radonjic, V. Begovic, B. Radovanovic, M. Mancic, Passive cooling of photovoltaic panel by aluminum heat sinks and numerical simulation, Ain Shams Eng. J. 15 (1) (2024) 102330, https://doi.org/10.1016/j.asej.2023.102330.
[14] Q. Luo, P. Li, L. Cai, X. Chen, H. Yan, H. Zhu, P. Zhai, P. Li, Q. Zhang, Experimental investigation on the heat dissipation performance of flared-fin heat sinks for concentration photovoltaic modules, Appl. Therm. Eng. 157 (2019) 113666, https://doi.org/10.1016/j.applthermaleng.2019.04.076.
[15] Y. Alihosseini, M. Zabetian Targhi, M.M. Heyhat, N. Ghorbani, Effect of a micro heat sink geometric design on thermo-hydraulic performance: A review, Appl. Therm. Eng. 170 (2020) 114974, https://doi.org/10.1016/j.applthermaleng.2020.114974.
[16] N. Bessanane, M. Si-Ameur, M. Rebay, Numerical study of the temperature effects on heat transfer coefficient in mini-channel pin-fin heat sink, Int. J. Heat Technol. 40 (1) (2022).
[17] A. Ahmed, G. Zhang, K. Shanks, S. Sundaram, Y. Ding, T. Mallick, Performance evaluation of single multi-junction solar cell for high concentrator photovoltaics using minichannel heat sink with nanofluids, Appl. Therm. Eng. 182 (2021) 115868, https://doi.org/10.1016/j.applthermaleng.2020.115868.
[18] A. Ahmed, K. Shanks, S. Sundaram, T.K. Mallick, Theoretical Investigation of the Temperature Limits of an Actively Cooled High Concentration Photovoltaic System, Energies 13 (8) (2020) 1902, https://doi.org/10.3390/en13081902.
[19] A.T. Okasha, F. Ghallab, T. Maatallah, N.A. Hassanain, A.K. Alghamdi, R. Zachariah, Numerical Study of Single-Layer and Stacked Minichannel-Based Heat Sinks Using Different Truncating Ratios for Cooling High Concentration Photovoltaic Systems, Sustainability 14 (9) (2022) 5352, https://doi.org/10.3390/su14095352.
[20] A. Torbatinezhad, M. Rahimi, A.A. Ranjbar, M. Gorzin, Performance evaluation of PV cells in HCPV/T system by a jet impingement/mini-channel cooling scheme, Int. J. Heat Mass Transf. 178 (2021) 121610, https://doi.org/10.1016/j.ijheatmasstransfer.2021.121610.
[21] M. Sadinezhad Fard, M. Rahimi, Y. Pahamli, H. Samadi, R. Bahrampoury, Cooling performance of sliver solar cells in low concentration PV system with ribbed-groove mini-channel heat sink, Int. J. Therm. Sci. 200 (2024) 108955, https://doi.org/10.1016/j.ijthermalsci.2024.108955.
[22] H. Ramezani, J. Bakhshi, M. Ghasemian, M. Sheikholeslami, A numerical investigation of the effect of a heat sink with sinusoidal fins on the performance of high-concentrated solar cells, Appl. Therm. Eng. 236 (2024) 121746, https://doi.org/10.1016/j.applthermaleng.2023.121746.
[23] T. Jatau, T. Bello-Ochende, A. Malan, Novel design of centralized square array of pin-fins in microchannels heat sink for thermal management of high concentrator photovoltaic system, Appl. Therm. Eng. 124943 (2024), https://doi.org/10.1016/j.applthermaleng.2024.124943.
[24] Y. Alihosseini, Y. Oghabneshin, A.R. Bari, S. Moslemi, A.R. Roozbehi, M.Z. Targhi, W. Guo, Performance of high-concentration photovoltaic cells cooled by a hybrid microchannel heat sink, Appl. Therm. Eng. 238 (2024) 122206, https://doi.org/10.1016/j.applthermaleng.2023.122206.
[25] A.M. Soliman, H. Hassan, S. Ookawara, An experimental study of the performance of the solar cell with heat sink cooling system, Energy Procedia 162 (2019) 127–135, https://doi.org/10.1016/j.egypro.2019.04.014.
[26] A.M. Soliman, H.H. Hassan, An experimental work on the performance of solar cell cooled by flat heat pipe, J. Therm. Anal. Calorim. 146 (2020) 1883–1892, https://doi.org/10.1007/s10973-020-10102-5.
[27] D.L. Evans, L.W. Florschuetz, Terrestrial concentrating photovoltaic power system studies, Sol. Energy 20 (1) (1978) 37–43.
[28] M. Khoshvaght-Aliabadi, M. Sahamiyan, M. Hesampour, O. Sartipzadeh, Experimental study on cooling performance of sinusoidal–wavy minichannel heat sink, Appl. Therm. Eng. 92 (2016) 50–61, https://doi.org/10.1016/j.applthermaleng.2015.09.015.
[29] P. Jiang, M. Fan, G. Si, Z. Ren, Thermal–hydraulic performance of small scale micro-channel and porous-media heat-exchangers, Int. J. Heat Mass Transfer 44 (5) (2001) 1039–1051, https://doi.org/10.1016/S0017-9310(00)00169-1.
[30] M. Rahimi, E. Karimi, M. Asadi, P. Valeh-e-Sheyda, Heat transfer augmentation in a hybrid microchannel solar cell, Int. Commun. Heat Mass Transfer 43 (2013) 131–137, https://doi.org/10.1016/j.icheatmasstransfer.2013.02.002.
[31] P. Valeh-e-Sheyda, M. Rahimi, E. Karimi, M. Asadi, Application of two-phase flow for cooling of hybrid microchannel PV cells: A comparative study, Energy Convers. Manage. 69 (2013) 122–130, https://doi.org/10.1016/j.enconman.2013.01.029.
[32] H.L. Luqman Azeez, A. Ibrahim, B.O. Omer Ahmed, A.H. Al-Waeli, M. Jaber, M. Aqil Afham Rahmat, Energy and exergy analysis of a novel collector design in a photovoltaic thermal system: An experimental study, Appl. Therm. Eng. 256 (2024) 124125, https://doi.org/10.1016/j.applthermaleng.2024.124125.
[33] B.O. Ahmed, A. Ibrahim, H.L. Azeez, S.S. Dol, A.H. Al-Waeli, M. Jaber, Energy and exergy analysis of a newly designed photovoltaic thermal system featuring ribs, petal array, and coiled twisted tapes: Experimental analysis, Case Stud. Therm. Eng. 63 (2024) 105388, https://doi.org/10.1016/j.csite.2024.105388.
[34] T. Wongwuttanasatian, T. Sarikarin, A. Suksri, Performance enhancement of a photovoltaic module by passive cooling using phase change material in a finned container heat sink, Sol. Energy 195 (2020) 47–53, https://doi.org/10.1016/j.solener.2019.11.053.
[35] P. Qi, D. Jing, Experimental and numerical study on the hydrothermal performances of a mirror Y-shaped convergent mini-channel heat sink, Case Stud. Therm. Eng. 53 (2024) 103966, https://doi.org/10.1016/j.csite.2023.103966.
[36] H. Xiao, Z. Liu, W. Liu, Conjugate heat transfer enhancement in the mini-channel heat sink by realizing the optimized flow pattern, Appl. Therm. Eng. 182 (2021) 116131, https://doi.org/10.1016/j.applthermaleng.2020.116131.
[37] E. Cuce, T. Bali, S.A. Sekucoglu, Effects of passive cooling on performance of silicon photovoltaic cells, Int. J. Low-Carbon Technol. 6 (2011) 299–308, https://doi.org/10.1093/IJLCT/CTR018.
[38] A. Elbreki, K. Sopian, A. Fazlizan, A. Ibrahim, An innovative technique of passive cooling PV module using lapping fins and planar reflector, Case Stud. Therm. Eng. 19 (2020) 100607, https://doi.org/10.1016/j.csite.2020.100607.
[39] M.R. Gomaa, W. Hammad, M. Al-Dhaifallah, H. Rezk, Performance enhancement of grid-tied PV system through proposed design cooling techniques: An experimental study and comparative analysis, Sol. Energy 211 (2020) 1110–1127, https://doi.org/10.1016/j.solener.2020.10.062.
[40] M. Sivashankar, C. Selvam, Experimental investigation on the thermal performance of low-concentrated photovoltaic module using various pin-fin configurations of heat sink with phase change materials, J. Energy Storage 55 (2022) 105575, https://doi.org/10.1016/j.est.2022.105575.
[41] S.N. Razali, A. Ibrahim, A. Fazlizan, M.F. Fauzan, R.K. Ajeel, E. Zairah Ahmad, W. E. Ewe, H.A. Kazem, Performance enhancement of photovoltaic modules with passive cooling multidirectional tapered fin heat sinks (MTFHS), Case Stud, Therm. Eng. 50 (2023) 103400, https://doi.org/10.1016/j.csite.2023.103400.